Missing Peroxy Radical Sources within a Rural Forest Canopy

Supplementary Information

G. M. Wolfe[1,*,**], C. Cantrell[2,***], S. Kim[2,****], R. L. Mauldin III[2,3,***], T. Karl[2,*****], P. Harley[2], A.Turnipseed[2], W. Zheng[2], F. Flocke[2], E. C. Apel[2], R. S. Hornbrook[2], S. R. Hall[2], K. Ullmann[2], S. B. Henry[1], J. P. DiGangi[1,******], E. S. Boyle[1], L. Kaser[4,*******], R. Schnitzhofer[4], A. Hansel[4], M. Graus[5], Y. Nakashima[6, ********], Y. Kajii[7], A.Guenther[2,********], and F. N. Keutsch[1]

[1]Department of Chemistry, University of Wisconsin, Madison, WI, USA

[2]Atmospheric Chemistry Division, National Center for Atmospheric Research, Boulder, CO, USA

[3]Department of Physics, University of Helsinki, Helsinki, Finland

[4]Institute of Ion Physics and Applied Physics, University of Innsbruck, Innsbruck, Austria

[5]Chemical Sciences Division, NOAA Earth System Research Laboratory, Boulder, CO, USA

[6]Division of Applied Chemistry, Faculty of Urban Environmental Sciences, Tokyo Metropolitan University, Tokyo, Japan

[7]Graduate School of Global Environmental Studies, Kyoto University, Kyoto, Japan

*Now at Joint Center for Earth Systems Technology, University of Maryland Baltimore County, Baltimore, MD, USA

**Now at Atmospheric Chemistry and Dynamics Laboratory, NASA Goddard Space Flight Center, Greenbelt, MD, USA

***Now at Department of Atmospheric and Oceanic Sciences, University of Colorado, Boulder, CO, USA

****Now at Department of Earth System Science, University of California, Irvine, CA, USA

*****Now at Institute for Meteorology and Geophysics, University of Innsbruck, Innsbruck, Austria

******Now at Department of Civil & Environmental Engineering, Princeton University, Princeton, NJ, USA

******* Now at Atmospheric Chemistry Division, National Center for Atmospheric Research, Boulder, CO, USA

******** Now at Department of Environmental and Natural Resource Science, Faculty of Agriculture, Tokyo University of Agriculture and Technology, Tokyo, Japan

*********Now at Atmospheric Sciences and Global Change Division, Pacific Northwest National Laboratory, Richland, WA USA

Table of Contents

Correction of MBO and Monoterpenes for In-Canopy Gradients

As mentioned in Sect. 2.3 of the main text, MBO and speciated monoterpene (MT) measurements were recorded at 25 m by the PTR-TOF-MS and TOGA instruments, respectively. It is preferable to constrain the model with these observations due to their temporal coverage (and speciation, in the case of MTs); however, as these species are directly emitted, they must first be corrected for the vertical gradient in mixing ratios. Figure S2 illustrates this correction, which involves three steps:

1) Mean diel cycles of MBO and total MT from the NCAR quadrupole PTR-MS at 4 m and 23 m are interpolated from their reporting interval of 90 min to the model time step of 30 min.
2) The ratio of measurements at these two heights is used to generate a time-dependent gradient correction factor.
3) This correction factor is applied to MBO (PTR-TOF-MS) and speciated MT (TOGA) observations at 25 m to estimate their within-canopy concentrations.

In-canopy gradients of these compounds can be significant, with correction factors ranging from 0.9 to 1.5 for MBO and from 1.2 to 1.8 for monoterpenes (Fig. S2).

Estimation of Model Uncertainty

Uncertainty in model-calculated mixing ratios arises mainly from confidence in observational constraints. The primary drivers of model-predicted peroxy radical concentrations in the present work are NO, VOCs, O_3, photolysis frequencies and OH (for scenarios where OH is constrained). Uncertainties for these measurements are listed in Table S1. To quantify the corresponding model uncertainty, a series of sensitivity runs were performed where each constraint was set to its lower or upper uncertainty limit while holding all other parameters at their nominal values. In the case of VOCs, including HCHO and CHOCHO, all constraints were taken simultaneously to their lower or upper limit (as opposed to a separate model run for each compound). Figure S3 shows the percentage change in HO_2*, RO_2*, total peroxy radicals and OH for each sensitivity experiment. Also shown is the total uncertainty, calculated by adding all of the upper and lower uncertainty limits in quadrature. For peroxy radicals, confidence in OH observations is the largest contributor to model uncertainty. Technically this contribution is absent when OH is not constrained to observations, which significantly decreases the total calculated uncertainty; however, we still use the total uncertainty from the base case as an upper limit for the uncertainty in the ModOH case. For OH, NO is the largest driver of uncertainty, followed by

VOC mixing ratios. The total uncertainties shown in Figure S3 correspond to error bars for model mixing ratios in the main text.

Model-Assisted Separation of HO_2 and RO_2 Measurements

As discussed in the main text, the signal from the nominal HO_2 channel (high NO/O_2 mode) of the PeRCIMS measurement likely includes a positive artifact due to fast conversion of certain organic peroxy radicals to HO_2. In particular, β-hydroxyalkylperoxy radicals, formed via OH-addition to alkenes, are known to cause such interferences (Fuchs et al., 2011;Hornbrook et al., 2011). Given that unsaturated biogenic hydrocarbons comprise a major fraction of reactive VOC during BEACHON-ROCS, we expect such radicals to be abundant in this environment. While the primary PeRCIMS observations of HO_2* and $HO_2 + RO_2$ provide a useful separation of the peroxy radical pool, it would be advantageous to also have an observational constraint on HO_2. Using 0-D box model results, we can explore potential corrections to the PeRCIMS measurements to obtain an estimate of ambient HO_2 mixing ratios. Here we investigate four calculations:

1) Correction of measured HO_2* with modeled β-hydroxyalkylperoxy radical concentrations;
2) Correction of measured $HO_2 + RO_2$ with the modeled $HO_2/(HO_2 + RO_2)$ ratio;
3) Correction of measured HO_2* with the modeled HO_2/HO_2* ratio; and
4) Correction of PeRCIMS sensitivities using the modeled RO_2 distribution.

The first three methods are relatively straightforward. Subtraction of modeled β-hydroxyalkylperoxy radicals from measured HO_2* is the simplest method, though this will overestimate HO_2 if the model underestimates concentrations of these radicals or if additional RO_2 also contribute to the HO_2* signal. The second and third calculations assume that the model adequately represents the relative distribution of peroxy radicals, even though absolute abundances are too low. This partitioning is largely controlled by the competition of HO_2 sinks via reaction with NO, HO_2 and RO_2. As noted in the main text (see e.g. Fig. 4), the $HO_2/(HO_2 + RO_2)$ ratio tends to decrease with higher peroxy radical levels, reflecting the somewhat faster rate of $RO_2 + HO_2$ relative to $HO_2 + HO_2$. In contrast, reaction with NO is less sensitive to the nature of the peroxy radical and forces this ratio to approach a value of 0.5 due to the fast cycling between RO_2, HO_2 and OH. Thus, since peroxy radicals are under-predicted during the day, we might expect the modeled $HO_2/(HO_2 + RO_2)$ ratio to be too high, resulting in an over-estimate of HO_2. Non-cycling radical sources (e.g. oVOC photolysis or decomposition of PAN-like compounds) could

also influence this estimate if they were sufficiently strong. Similar qualifications hold for the HO_2/HO_2* method. Additionally, this calculation is tied to our assumptions regarding which RO_2 to include in the model HO_2* family. A list of these species is provided in Table S2.

The last method is more sophisticated as it involves manipulation of raw instrument signals. Following equations (5) – (12) of Hornbrook et al. (2011), the PeRCIMS signals in low and high NO/O_2 modes are related to ambient concentrations as

$$S_{low}F_{low} = [HO_2] + \alpha_{low}[RO_2] \quad \text{(S1)}$$

$$S_{high}F_{high} = [HO_2] + \alpha_{high}[RO_2] \quad \text{(S2)}$$

Here, *S* is the background-corrected instrument signal, *F* is the calibrated sensitivity to HO_2, and α is the empirically-determined ratio of the calibration factor for RO_2 relative to that for HO_2. By default, concentrations of HO_2 and HO_2 + RO_2 are calculated by inverting these equations and using the α values determined for CH_3O_2 (α_{low} = 1.22, α_{high} = 0.17). We can improve upon this calculation by estimating α as the weighted sum of contributions from each RO_2:

$$\alpha_{weighted} = \sum_i \alpha_i [RO_2]_i / \sum_i [RO_2]_i \quad \text{(S3)}$$

Unfortunately, α values have only been determined for a handful of peroxy radicals, mostly those derived from anthropogenic alkanes and alkenes (Hornbrook et al., 2011). For this analysis, we assume that all β-hydroxyalkylperoxy radicals (Table S2) exhibit the same sensitivity as isoprene (α_{low} = 1.18, α_{high} = 1.12), while other RO_2 behave like CH_3O_2. Using the RO_2 distribution from the base model simulation (Fig. 4), we calculate new values (averaged over 24 hours) of α_{low} = 1.201 ± 0.001 and α_{high} = 0.61 ± 0.02. Equations (S1) and (S2) are first used to deconvolute $S_{low}F_{low}$ and $S_{high}F_{high}$ from observations (using α-values for CH_3O_2). New concentrations for HO_2 and HO_2 + RO_2 are then calculated with the weighted α-values.

Figure S6 compares the HO_2 and RO_2 mixing ratios calculated from all methods with the measured HO_2* and RO_2*. Note that total peroxy radical concentrations remain the same in all cases. The first three methods decrease HO_2 to near or just below the lower uncertainty limit throughout the day, though the decrease is relatively smaller at midday for the β-RO_2 subtraction (first) method. HO_2 derived from these corrections generally maintains the same diel shape as HO_2*, though from the changes to RO_2 it is clear that these methods preferentially shift HO_2 into RO_2 at noontime, with

comparatively smaller changes in the afternoon. HO_2 estimated via the sensitivity correction (fourth) method is similar to that from the ratio-scaling methods at mid-day but significantly lower in the morning and afternoon. The profile of this corrected HO_2 seems unexpectedly sharp, especially when considering other observations such as OH concentrations. This may indicate that 1) the model over-predicts the contribution of β-hydroxyalkylperoxy radicals to total RO_2 at these times, or 2) it is not appropriate to use isoprene-peroxy radicals as a proxy for all β-hydroxyalkylperoxy radicals. In either case, the accumulation of uncertainties from measurements and model results makes it difficult to utilize the derived HO_2 and RO_2 mixing ratios with sufficient confidence.

References

Apel, E. C., Emmons, L. K., Karl, T., Flocke, F., Hills, A. J., Madronich, S., Lee-Taylor, J., Fried, A., Weibring, P., Walega, J., Richter, D., Tie, X., Mauldin, L., Campos, T., Weinheimer, A., Knapp, D., Sive, B., Kleinman, L., Springston, S., Zaveri, R., Ortega, J., Voss, P., Blake, D., Baker, A., Warneke, C., Welsh-Bon, D., de Gouw, J., Zheng, J., Zhang, R., Rudolph, J., Junkermann, W., and Riemer, D. D.: Chemical evolution of volatile organic compounds in the outflow of the Mexico City Metropolitan area, Atmos. Chem. Phys., 10, 2353-2375, 2010.

DiGangi, J. P., Boyle, E. S., Karl, T., Harley, P., Turnipseed, A., Kim, S., Cantrell, C., Maudlin Iii, R. L., Zheng, W., Flocke, F., Hall, S. R., Ullmann, K., Nakashima, Y., Paul, J. B., Wolfe, G. M., Desai, A. R., Kajii, Y., Guenther, A., and Keutsch, F. N.: First direct measurements of formaldehyde flux via eddy covariance: implications for missing in-canopy formaldehyde sources, Atmospheric Chemistry and Physics, 11, 10565-10578, 2011.

Fuchs, H., Bohn, B., Hofzumahaus, A., Holland, F., Lu, K. D., Nehr, S., Rohrer, F., and Wahner, A.: Detection of HO_2 by laser-induced fluorescence: calibration and interferences from RO_2 radicals, Atmos. Meas. Tech., 4, 1209-1225, 2011.

Graus, M., Muller, M., and Hansel, A.: High Resolution PTR-TOF: Quantification and Formula Confirmation of VOC in Real Time, Journal Of The American Society For Mass Spectrometry, 21, 1037-1044, 2010.

Hornbrook, R. S., Crawford, J. H., Edwards, G. D., Goyea, O., Maudlin III, R. L., Olson, J. S., and Cantrell, C. A.: Measurements of tropospheric HO_2 and RO_2 by oxygen dilution modulation and chemical ionization mass spectrometry, Atmos. Meas. Tech., 4, 735-756, 10.5194/amt-4-735-2011, 2011.

Hottle, J. R., Huisman, A. J., Digangi, J. P., Kammrath, A., Galloway, M. M., Coens, K. L., and Keutsch, F. N.: A Laser Induced Fluorescence-Based Instrument for In-Situ Measurements of Atmospheric Formaldehyde, Environ. Sci. Technol., 43, 790-795, 2009.

Huisman, A. J., Hottle, J. R., Coens, K. L., DiGangi, J. P., Galloway, M. M., Kammrath, A., and Keutsch, F. N.: Laser-induced phosphorescence for the in situ detection of glyoxal at part per trillion mixing ratios, Anal. Chem., 80, 5884-5891, 2008.

Karl, T., Apel, E., Hodzic, A., Riemer, D. D., Blake, D. R., and Wiedinmyer, C.: Emissions of volatile organic compounds inferred from airborne flux measurements over a megacity, Atmos. Chem. Phys., 9, 271-285, 2009.

Sadanaga, Y., Yoshino, A., Watanabe, K., Yoshioka, A., Wakazono, Y., Kanaya, Y., and Kajii, Y.: Development of a measurement system of OH reactivity in the atmosphere by using a laser-induced pump and probe technique, Rev. Sci. Instr., 75, 2648-2655, 2004.
Shetter, R., Junkermann, W., Swartz, W., Frost, G., Crawford, J., Lefer, B., Barrick, J., Hall, S., Hofzumahaus, A., Bais, A., Calvert, J., Cantrell, C., Madronich, S., Muller, M., Kraus, A., Monks, P., Edwards, G., McKenzie, R., Johnston, P., Schmitt, R., Griffioen, E., Krol, M., Kylling, A., Dickerson, R., Lloyd, S., Martin, T., Gardiner, B., Mayer, B., Pfister, G., Roth, E., Koepke, P., Ruggaber, A., Schwander, H., and van Weele, M.: Photolysis frequency of NO2: Measurement and modeling during the International Photolysis Frequency Measurement and Modeling Intercomparison (IPMMI), Journal of Geophysical Research-Atmospheres, 108, 10.1029/2002JD002932, 2003.
Slusher, D. L., Huey, L. G., Tanner, D. J., Flocke, F. M., and Roberts, J. M.: A thermal dissociation-chemical ionization mass spectrometry (TD-CIMS) technique for the simultaneous measurement of peroxyacyl nitrates and dintrogen pentoxide, J. Geophys. Res., 109, 10.1029/2004JD004670, 2004.
Tanner, D. J., Jefferson, A., and Eisele, F. L.: Selected ion chemical ionization mass spectrometric measurement of OH, J. Geophys. Res. Atmos., 102, 6415-6425, 1997.
Wolfe, G. M., Thornton, J. A., McKay, M., and Goldstein, A. H.: Forest-atmosphere exchange of ozone: sensitivity to very reactive biogenic VOC emissions and implications for in-canopy photochemistry, Atmos. Chem. Phys., 11, 7875-7891, 2011.

Table S1. BEACHON-ROCS 2010 observations used in this study

Parameter	Instrument/Technique[a]	Uncertainty	Height (m)	Reference
HO_2, $RO_2 + HO_2$	PeRCIMS	35%	1.6	(Hornbrook et al., 2011)
OH	CIMS	35%	1.6	(Tanner et al., 1997)
OH reactivity	Laser pump-probe LIF	5%	4	(Sadanaga et al., 2004)
NO	Chemiluminescence	15%	2	Eco Physics CLD 88 p
NO_2	Conversion to NO	15%	2	Droplet Technologies Blue Light Converter
O_3	UV absorption	2%	2	2B Technology
CO	IR absorption	15%	3	Thermo Scientific Model 48i
VOC	PTRMS-TOF[b]	15%	25	(Graus et al., 2010)
	TOGA (Gas Chromatography)[c]	15%	25	(Apel et al., 2010)
	PTRMS-Quad[d]	15%	2.3, 23	(Karl et al., 2009)
HCHO	LIF	20%	9	(Hottle et al., 2009) (DiGangi et al., 2011)
Glyoxal	Laser-Induced Phosphorescence	20%	2	(Huisman et al., 2008)
PAN, PPN	Thermal Dissociation CIMS	20%	25	(Slusher et al., 2004)
$J(NO_2)$	Filter Radiometer	11%	2, 25[e]	(Shetter et al., 2003)
T, P, RH	-	-	2	Vaisala WXT-520

[a]CIMS: chemical ionization mass spectrometry; LIF: laser-induced fluorescence; PTRMS: proton transfer mass spectrometry; TOF: time-of-flight.
[b]Includes MBO, benzene, toluene and acetaldehyde.
[c]Includes isoprene, α-pinene, β-pinene, limonene, camphene, non-speciated monoterpenes, acetone, methanol, methyl vinyl ketone, methacrolein, propanal, n-butanal and 1,3-butadiene.
[d]MBO and total monoterpene gradients used to correct PTRMS-TOF and gas chromatography data (see text for details).
[e]Measured downwelling $J(NO_2)$ multiplied by 1.05 to account for upwelling radiation as determined from a single day of observations.

Table S2. Contribution of model species to HO_2*

Species	**Parent VOC**	**% of HO_2*[a]**
HO2	-	62.2
MBOAO2 MBOBO2	MBO	22.7
ISOPAO2 ISOPBO2 ISOPCO2 ISOPDO2	Isoprene	4.5
APINAO2 APINBO2 APINCO2	α-pinene	0.8
BPINAO2 BPINBO2 BPINCO2	β-pinene	2.8
LIMAO2 LIMBO2 LIMCO2	Limonene	2.3
LIMALO2 LIMALAO2 LIMALBO2	Limonal	2.7
MTO2	Camphene, Unspeciated MT	0.6
HMVKAO2 HMVKBO2	MVK	1.1
MACRO2 MACROHO2	MACR	0.1
BUTDBO2 BUTDCO2	Butadiene	0.1
ACO3B	Acrolein	0.01
BZBIPERO2	Benzene	0.003
PHENO2	Phenol	0.0005
TLBIPERO2	Toluene	0.04
CRESO2	Cresol	0.002

[a]24-hour average from base model simulation.

Table S3. Very reactive VOC reaction mechanism

Reaction[a]	**k(298K)**[b] **(cm^3 $molec^{-1}$ s^{-1})**	**Notes**
VRVOC + OH → VRO21	2.0×10^{-10}	-
VRVOC + O3 → 0.1VRO22 + 0.1OH + 0.9VROX	1.2×10^{-14}	Assumes 10% radical yield
VRVOC + NO3 → 0.9VRO23 + 0.1VROX	2.2×10^{-11}	Assumes 10% alkyl nitrate yield
VRO2n + NO → VROX + 0.76NO2 + 0.76HO2	9.0×10^{-12}	Assumes 24% alkyl nitrate yield
VRO2n + HO2 → VROX	2.1×10^{-11}	-
VRO2n + RO2 → VROX + 0.7HO2	9.0×10^{-14}	-

[a]Reactions follow Wolfe et al. (2011), except that initial VRO2 are speciated according to oxidant. All VRO2 are assigned the same loss processes. VROX is a generic oxidized product that does not undergo further chemistry.
[b]Rate constants are equal to those of β-caryophyllene for VRVOC and BPINAO2 for VRO2.

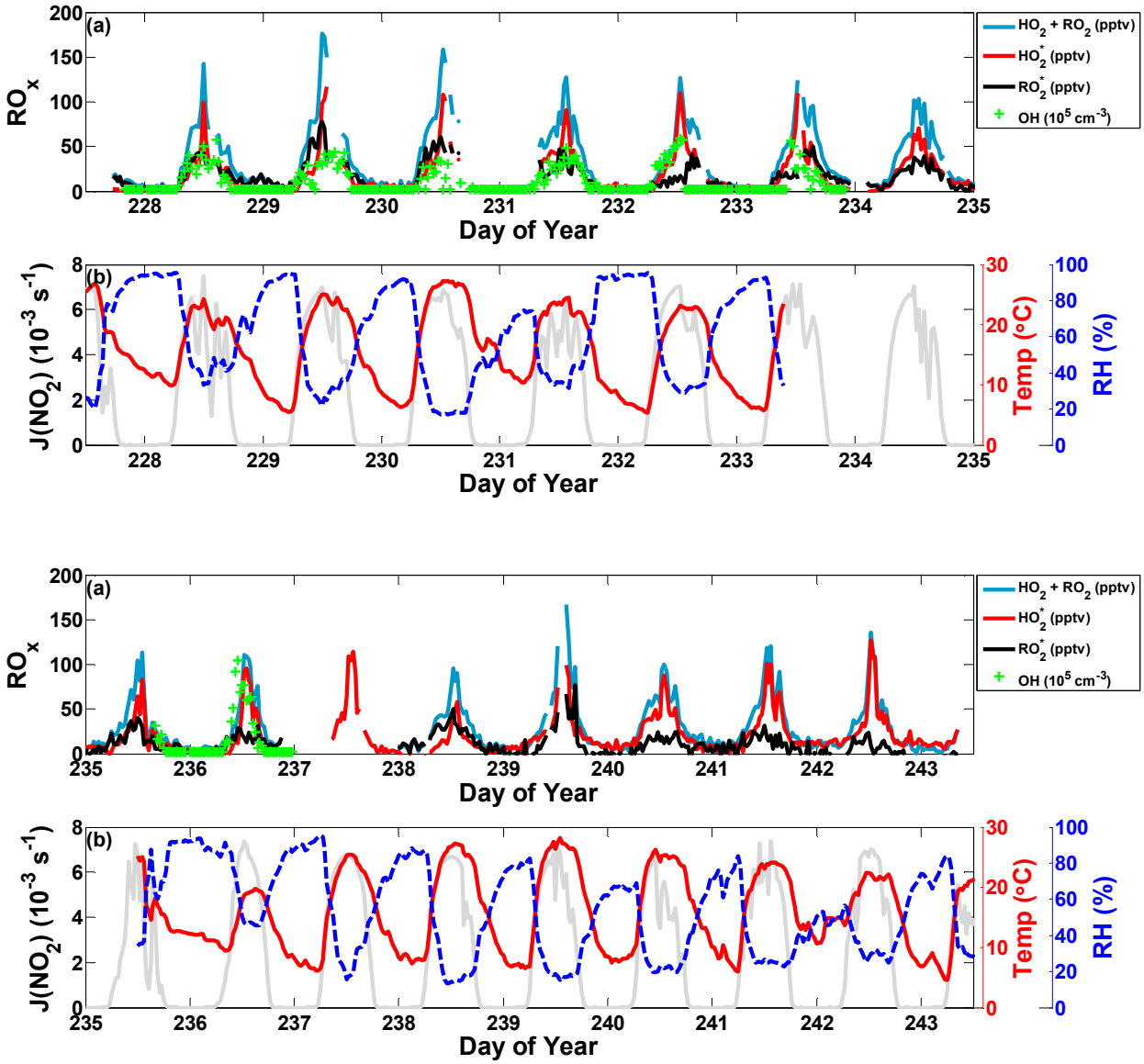

Figure S1. Full time series for observations of peroxyl radicals and meteorology during BEACHON-ROCS. (a) Total peroxyl radicals (blue line), HO_2* (green line), RO_2* (black line) and OH (green crosses). Peroxy radicals units are pptv, and OH units are 10^5 molec cm^{-3}. (b) Above-canopy NO_2 photolysis frequencies (gray solid line), air temperature (red solid line) and relative humidity (blue dashed line). All data are displayed as 30-minute averages. OH values below the instrument detection limit (5 x 10^5 cm^{-3}) are nominally set to half of this value.

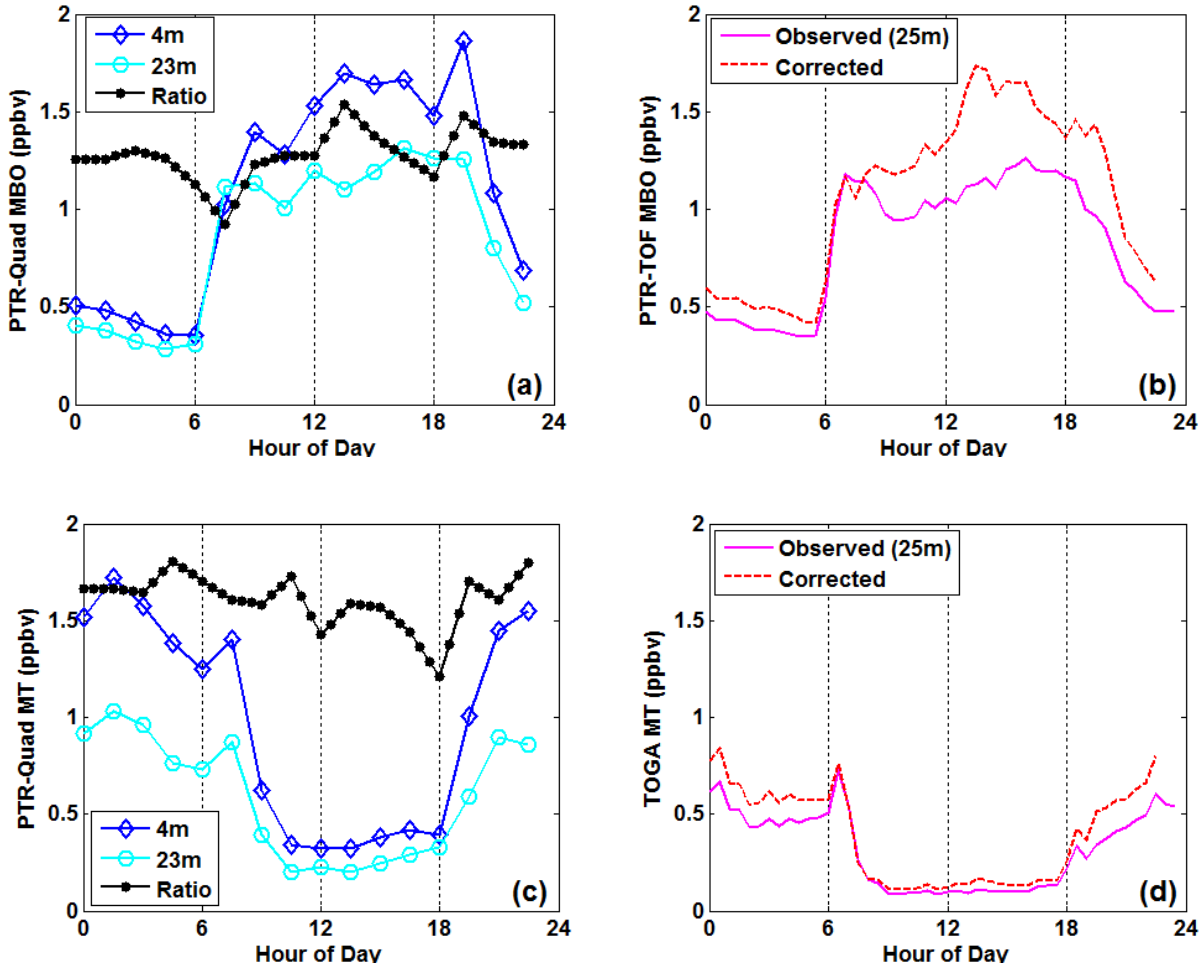

Figure S2. Demonstration of vertical gradient corrections for MBO (a, b) and monoterpenes (c, d). The left panels show diurnal mean observations of MBO and total monoterpenes from the PTR-quadrupole instrument, with inlet heights at 4m (blue diamonds) and 23 m (cyan circles). Also shown is the ratio of the 4m measurement to the 23m measurement, which defines the correction factor described in the SI text. The right panels show observations of MBO and total monoterpenes taken at 25m via the PTR-TOF and TOGA instruments, respectively. Total monoterpenes represent the sum of α-pinene, β-pinene, 3-carene, myrcene, limonene, 1,8-cineole, camphene and a group of unspeciated monoterpenes. Observations (solid magenta line) are multiplied by the correction factor to give gradient-corrected values (dashed red line), which are used in model calculations.

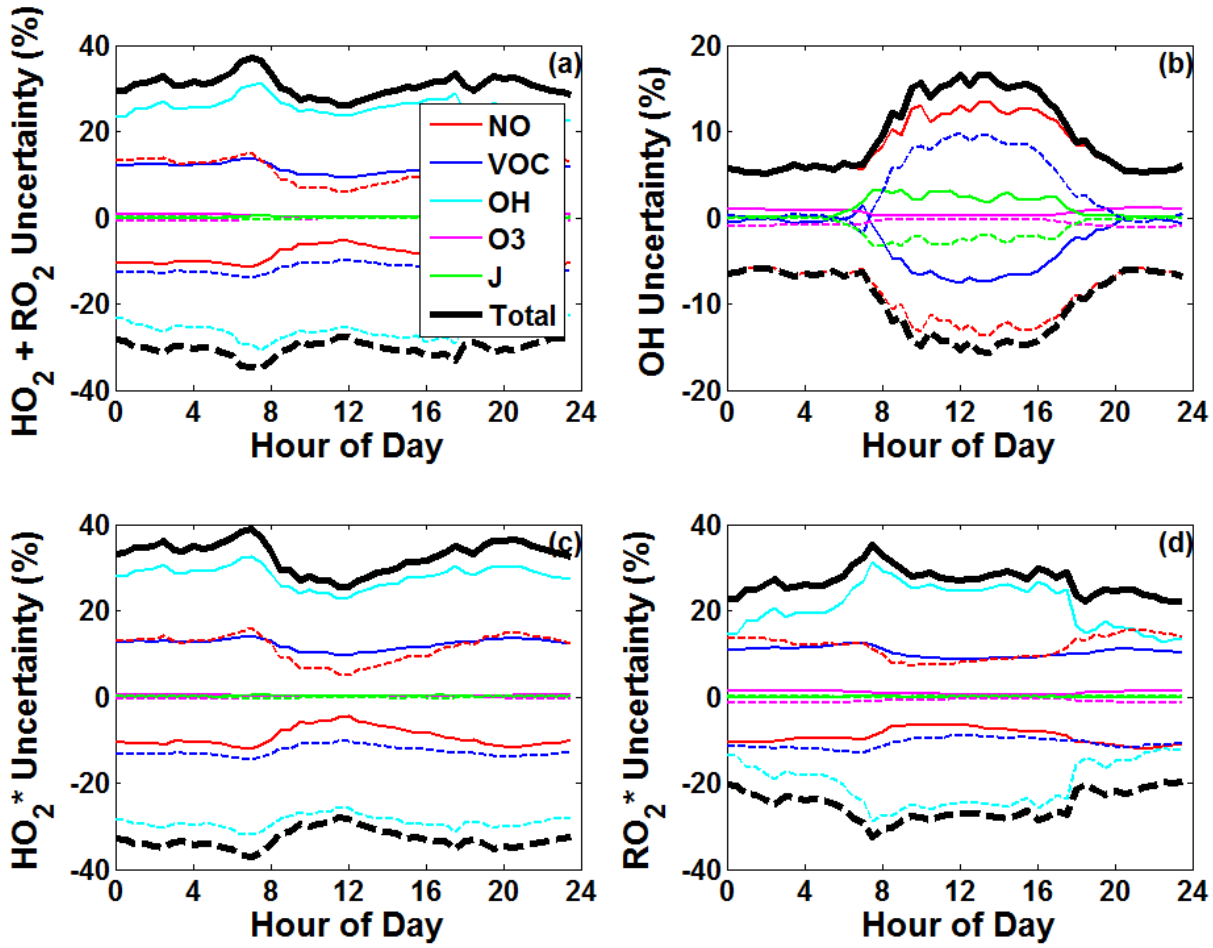

Figure S3. Results of sensitivity runs for estimating model uncertainty stemming from observational constraints for (a) total peroxy radicals, (b) OH, (c) HO_2* and (d) RO_2*. Thin lines represent percentage change in modeled concentrations when setting each listed species (NO, VOC, OH, O3, or photolysis frequencies) to their upper (solid lines) or lower (dashed lines) limits. For peroxy radicals, the base model scenario is used as the reference case, while for OH the "ModOH" scenario is used. Thick black lines denote the total uncertainty, calculated by summing up all positive or negative uncertainties in quadrature.

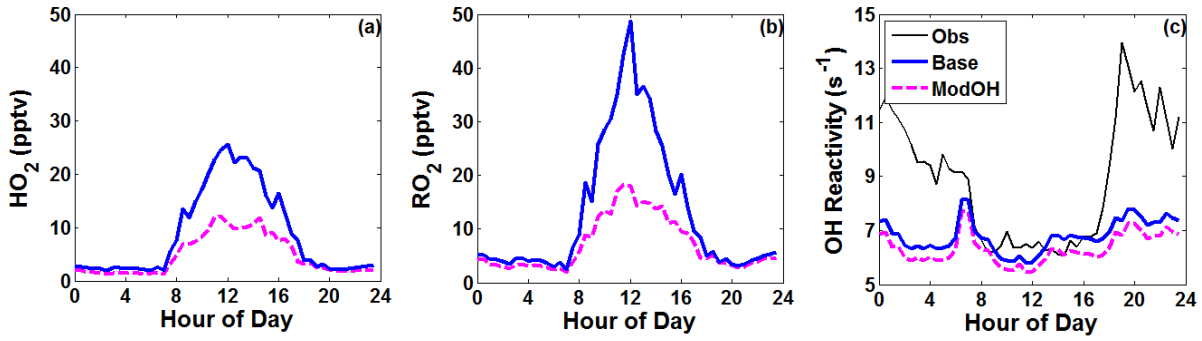

Figure S4. Additional 0-D model results: (a) HO_2, (b) total RO_2 and (c) OH reactivity. Model results are shown for the base scenario (solid blue line) and ModOH scenario (dashed magenta line). Total observed OH reactivity is also shown (solid black line). Total RO_2 represents the sum of 347 model species. Modeled OH reactivity is calculated by summing the loss rate of OH from all relevant reactions (1014 total) and dividing by the OH concentration.

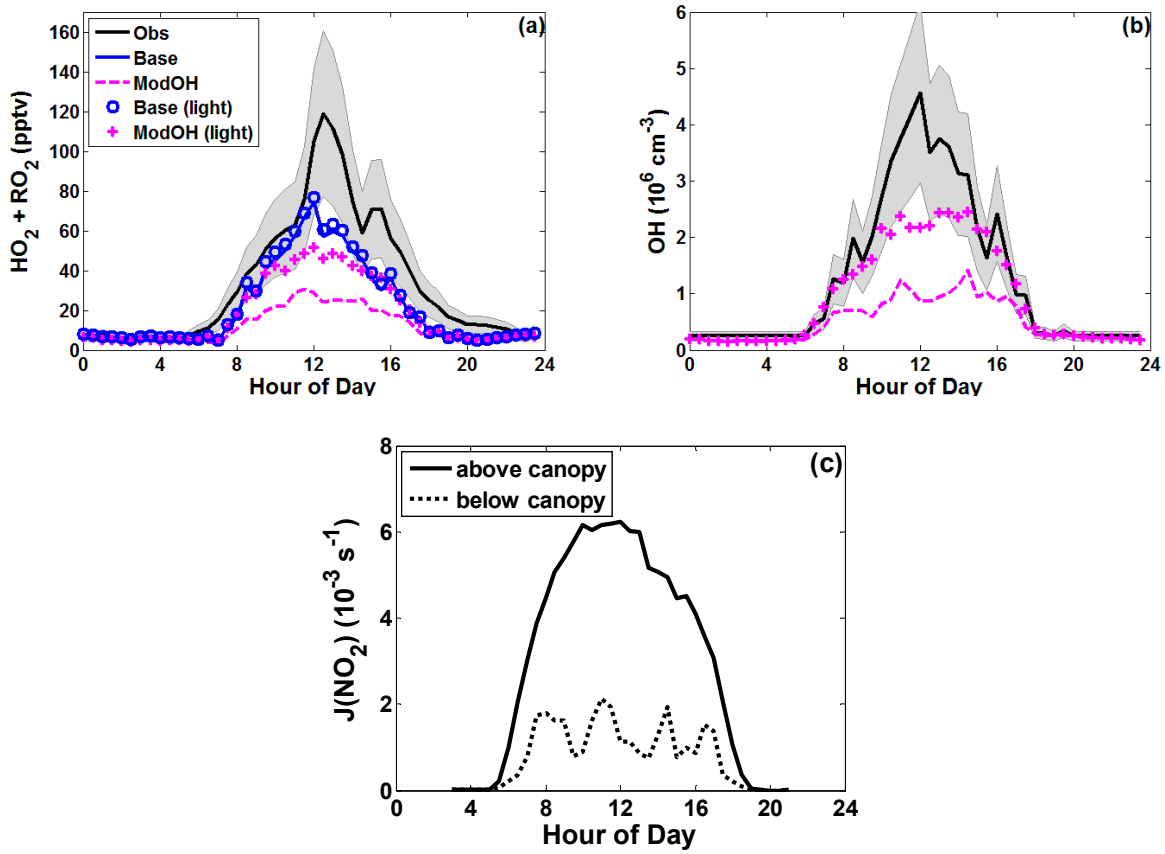

Figure S5. Comparison of model output for (a) total peroxy radicals and (b) OH concentrations under varying sunlight conditions. Solid black lines with shaded gray areas represent observations and their associated uncertainties. Colored lines denote model results with photolysis frequencies constrained by below-canopy $J(NO_2)$ measurements and include the base (solid blue line) and ModOH (dashed magenta line) scenarios. Symbols denote results for scenarios constrained by $J(NO_2)$ measured above the canopy (blue circles: base, magenta crosses: ModOH). Observed NO_2 photolysis frequencies are also shown (c).

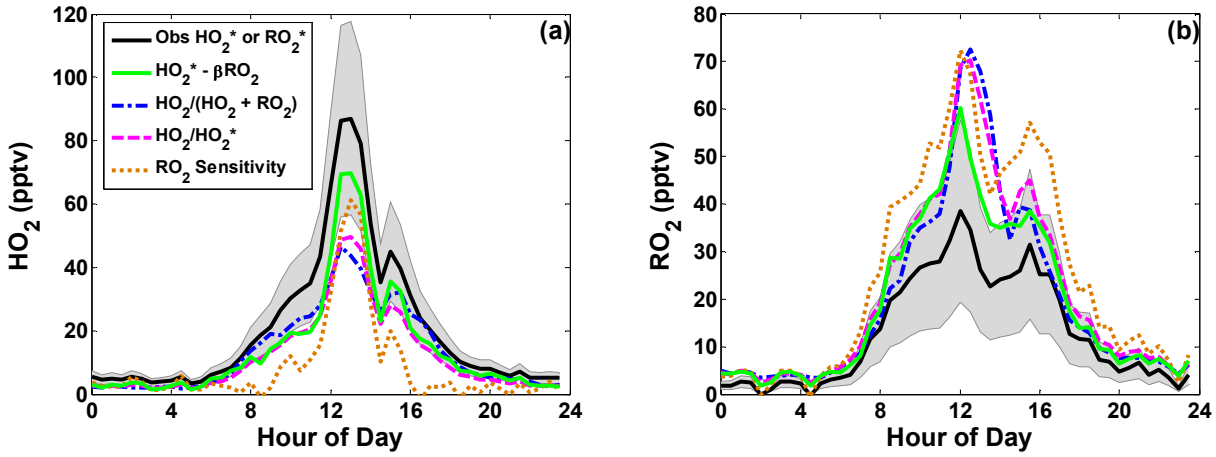

Figure S6. Comparison of model-assisted corrections to peroxy radical observations. Black lines with shaded areas denote observations and their associated uncertainties; note that the RO_2 uncertainty is 50% due to combined uncertainties of the HO_2* and HO_2 + RO_2 measurements (35% each). Correction methods include subtraction of modeled β-hydroxyalkylperoxy radicals (solid green line), scaling by modeled $HO_2/(HO_2 + RO_2)$ (dash-dotted blue line), scaling by modeled HO_2/HO_2* (dashed magenta line) and correction of PeRCIMS sensitivities with the modeled RO_2 distribution (dotted orange line).

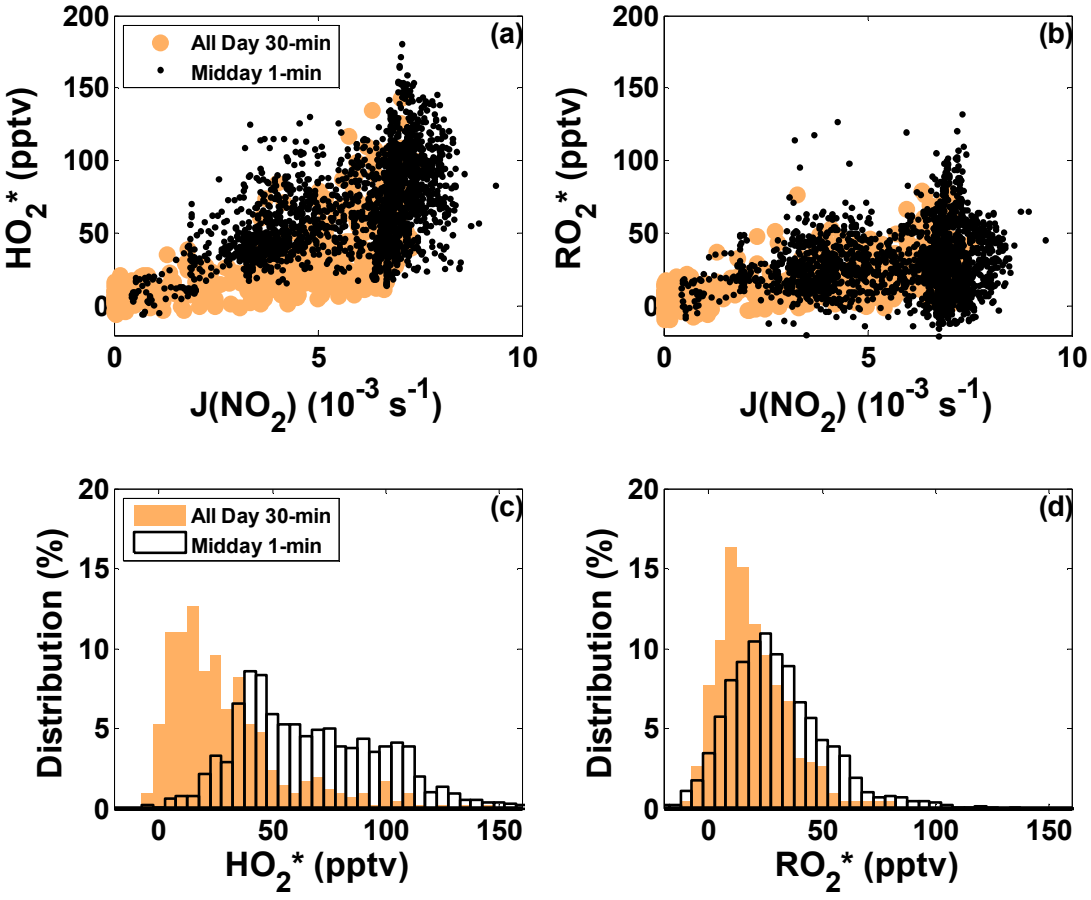

Figure S7. (a-b) Scatter plots of observed peroxy radical mixing ratios and NO_2 photolysis frequencies (a proxy for solar radiation). Orange circles represent all daytime data ($J(NO_2) > 2 \times 10\text{-}6\ s^{-1}$), averaged to 30 minute intervals to effectively damp out fast changes. Black points represent 1 minute averaged data from hours 11:30 to 14:30 only. Correlation coefficients (r^2) for scatter plots are 0.41 and 0.26 for HO_2* 30-min and 1-min and 0.30 and 0.03 for RO_2* 30-min and 1-min, respectively. (c-d) Distribution of peroxy radical mixing ratios for all 30 minute averaged daytime data (solid orange) and 1 minute averaged midday data (black outline).

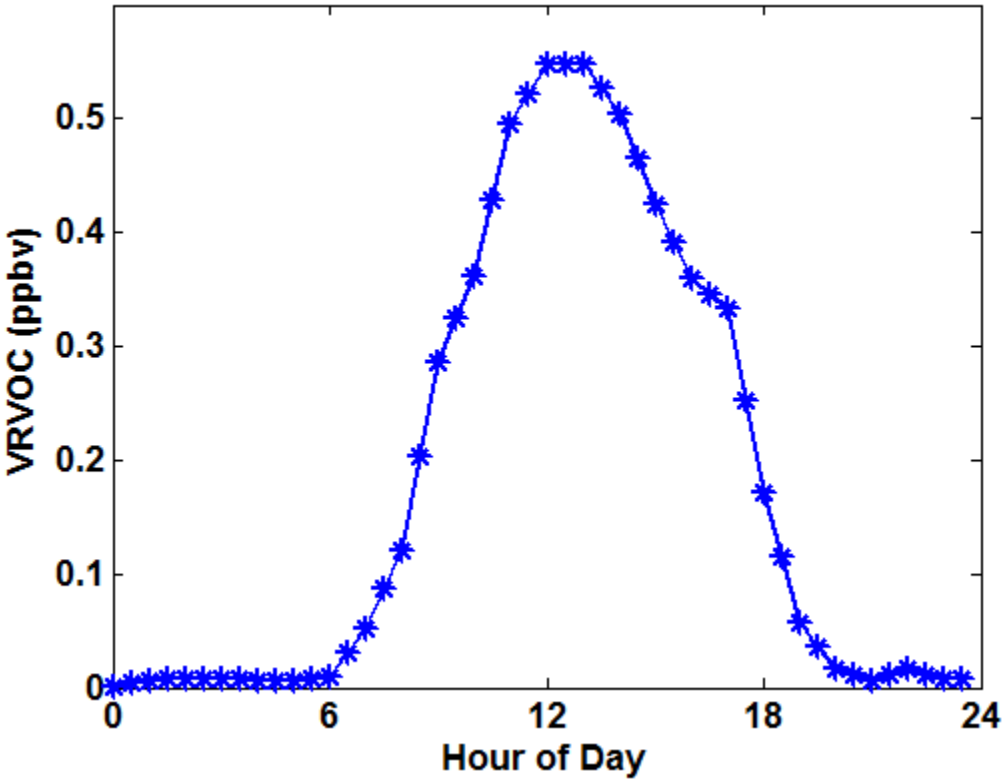

Figure S8. Mixing ratio of very reactive VOC (VRVOC) used to constrain the model scenario described in section 5.2 of the main text.